COMMUNICATION

Check for updates

Solvation directed morphological control in metal oxide nanostructures†

Duo Song,‡ Lili Liu,‡ Andrew Ritchhart and Maria L. Sushko ⓘD *

The development of structural hierarchy on various length scales during the crystallization process is ubiquitous in biological systems and minerals and is common in synthetic nanomaterials. The driving forces for the formation of complex architectures range from local interfacial interactions, that modify interfacial speciation, local supersaturation, and nucleation barriers, to macroscopic interparticle forces. Although it is enticing to interpret the formation of hierarchical architectures as the assembly of independently nucleated building blocks, crystallization pathways often follow monomer-by-monomer addition with structural complexity arising from interfacial chemical coupling and strongly correlated fluctuation dynamics in the electric double layers. Here, we show that the development of structural hierarchy through heterogeneous nucleation is driven by dipolar and solvation forces. Specifically, coupled simulations and experimental studies revealed that dipole build-up along the slow growth direction can trigger twinning and the development of branched architectures. Enthalpic solvation interactions were shown to either enhance or reduce the dipole moment of the nanoparticles and, thereby, control crystal morphology and architecture. The systematic studies of chemical coupling between different solvents and undercoordinated surface atoms of the growing nanocrystals revealed the mechanism of dimensionality control and the development of structural hierarchy without ligands or structure-directing agents.

1. Introduction

Morphological control during nanoparticle synthesis can be achieved using several conceptually different approaches. The most common method is to leverage face-specific ligand adsorption.[1–3] The adsorbed ligands direct the growth of specific faces by modifying their relative surface energies. These changes in surface energies can be finely tuned through ligand chemistry and surface density, providing a flexible approach to controlling particle morphology.[4,5] Ligands used as face-specific capping agents can direct the formation of well-defined nanostructures. For example, preferential adsorption onto the (100) crystal faces of the fcc crystals can create (100)-plane-stabilized nanocubes, and capping the (111) crystal faces can yield octahedrons surrounded by the (111)-planes.[1,2] Capping a specific crystal facet could also promote overgrowth at a certain site or inhibit the growth of a certain crystal surface, forming a defect-rich concave structure.[6–8]

Alternatively, tuning the chemical potential of precursor species by changing synthesis parameters, such as precursor concentration, chemical identity of counterions, and solvent, proved to be a powerful approach to direct growth and crystal morphology. For example, numerous studies report the switching between classical monomer-by-monomer growth and particle-based crystallization caused by changing precursor concentration or pH.[9–14] The associated crystal morphologies reflect the differences in the growth mechanism. However, the transitions between faceted crystals, plate- and rod-like morphologies, and hierarchical architectures are often difficult to trace back to interfacial forces and the potential of mean-force of precursor species.[15]

When the growth pathway involves heterogeneous nucleation and monomer-by-monomer addition, as observed in ZnO,[16,17] branching implies a deviation of the structure of the growing crystal from its ideal bulk atomic arrangement. Therefore, it is worth investigating if the deviations from the bulk structure and properties of the nucleated nanoparticles might provide clues about the mechanism for branching. Even when the nucleus is crystalline, quantum confinement and reduced dielectric screening at the nanoscale modulate its surface and volume properties. Due to these unique electronic properties, small deviations from the bulk-like positions of surface atoms and small distortions of the unit cell of nano-

Pacific Northwest National Laboratory, Richland, WA, USA.
E-mail: maria.sushko@pnnl.gov (Maria Sushko)

crystals can lead to dipole moments of several Debyes.[15] Furthermore, for materials with polar faces, the common macroscopic mechanisms of dipole compensation *via* surface reconstruction and defect formation or ligand and solvent adsorption are less efficient at the nanoscale because surface reconstruction becomes thermodynamically unfavorable and fluctuations in ligand distributions on nanoparticle faces are translated into significant fluctuations in the surface dipole and into buildup of inner potential.[18] These fluctuations in ligand coverage can leave surface dipoles partially uncompensated and induce dipoles on nonpolar surfaces.[19] Therefore, nanoparticles often have a dipole moment that can drive their assembly into linear one-dimensional (1D) chain-like structures[20] or the formation of nanorods along the direction of the particle dipoles, *e.g.*, along the ⟨001⟩ direction for ZnO.[21,22] Dipolar forces can also be responsible for redirecting the growth of nanoparticles toward branching when the dipole builds up on some of the nanoparticle faces during growth.[23] Here, we aim to understand how nanoscale dipolar interactions can be controlled to direct growth pathways and crystal dimensionality. We also address the mechanism of structural hierarchy development through branching when the growth does not involve oriented attachment or structure-directing agents.[15,17] Understanding the branching mechanism can help control the crystal's architecture and dimensionality during the post-nucleation stage exclusively by tuning the interfacial forces in the electric double layer of the nucleus.

2. Results and discussion

2.1. Dipole build-up during nanoparticle growth

The surface structure of nanoparticles reflects the interplay between the interfacial energy of the corresponding crystal faces and the contribution from interfacial solvation. These properties of the corresponding infinite solid–liquid interfaces are insufficient to capture the essential contributions to surface energy. The finite nature of nanoparticles is manifested in the deviation of the structure and electronic properties of nanoparticle faces from the corresponding extended surfaces. These effects were studied here using ZnO as a model ionic material known to produce a variety of complex nanoarchitectures. The experiments and calculations were performed in pure solvents with different interactions with ZnO faces to eliminate the impact of face-specific binding of ligands.

Our previous studies demonstrated that ZnO grows faceted nanorods in an aqueous solution, which subsequently evolves into a branched architecture with self-similar nanorod branches.[16] Detailed *in situ* studies revealed that ZnO branching in aqueous solution is not the result of particle-based crystallization. Instead, the branched ZnO nanorod growth follows the monomer-by-monomer pathway with branching involving the formation of twin boundaries at the (10$\bar{1}$0) surfaces.[16] To understand the mechanism of twinning the structure of a nanorod with a representative cross-section was simulated

using a novel hybrid approach based on density functional theory (DFT).[24,25] The approach overcomes the limited reach of molecular simulation methods into relevant scales of time, length, and system complexity. The novel hybrid approach couples first-principles plane-wave DFT with classical DFT (cDFT). In this approach, a region of interest, including the ZnO nanoparticle and its first solvation layer, is described using DFT, which interacts with the surrounding medium described using cDFT to arrive at a self-consistent ground state. Benchmarking against experimental observations and entirely first-principle DFT simulations demonstrates that this hybrid model efficiently encompasses the key short-range and collective interactions in the electric double layer and interfacial relaxation of solid/liquid interfaces.[24] The ZnO nanorod was generated from the wurtzite phase of bulk ZnO crystal with lattice parameters of a = 3.25 Å, and c = 5.201 Å (see ESI† for details).[23,26,27] Solution model mirrored the experimental composition of 2.5 mM $Zn(NO_3)_2$ and 38 mM KOH in water, ethylene glycol, or ethanol. Simulations revealed a significant relaxation of Zn–O dimers at the side surfaces, with Zn atoms moving inward away from their bulk-like position by 0.36 Å. The surface Zn–O dimer, on average, formed a 9.4-degree angle with the surface (Fig. 1A). Each of these Zn–O dimers carries a 7.14D dipole, which builds up with the elongation of the nanorod. Dipole build-up reflects the nanoscale nature of the particles, in which quantum confinement prevents the creation of the space charge layer to compensate for surface dipoles.[23]

2.2. Solvent effect on dipolar interactions

Partial dipole compensation may be achieved through interactions with a polar solvent. It is reasonable to assume that solvation water will effectively compensate surface dipole of the nanoparticle. Surprisingly, DFT results indicate that hydration water not only does not compensate surface dipole but enhances it by binding to surface Zn atoms and forming hydrogen bonds with surface O (Fig. 1B and C). The resulting average angle formed by the surface Zn–O dimers increases from 9.4° degrees in vacuum to 20.4° degrees in water.

This dipole enhancement in an aqueous solution leads to dipole accumulation along the side surfaces of the ZnO nanorod with the elongation of the nanorod. The associated thermodynamic cost of dipole accumulation prevents further elongation of the nanorod. In the absence of other mechanisms for dipole compensation, such as the formation of the space-charge layer or ligand adsorption, the formation of twin boundaries and redirection of the growth towards branching on one hand compensates the surface dipole at the twin boundary sites and preserve thermodynamically favorable fast growth direction along [001] axis for each branch. As reported previously, the growth process yields the formation of branched architecture with self-similar shapes of the parent particles and the branches (Fig. 1C inset).[16]

We systematically varied the solvent chemistry to demonstrate the effect of solvation on dipolar interactions and the morphology of nanoparticles. Specifically, ethylene glycol (EG)
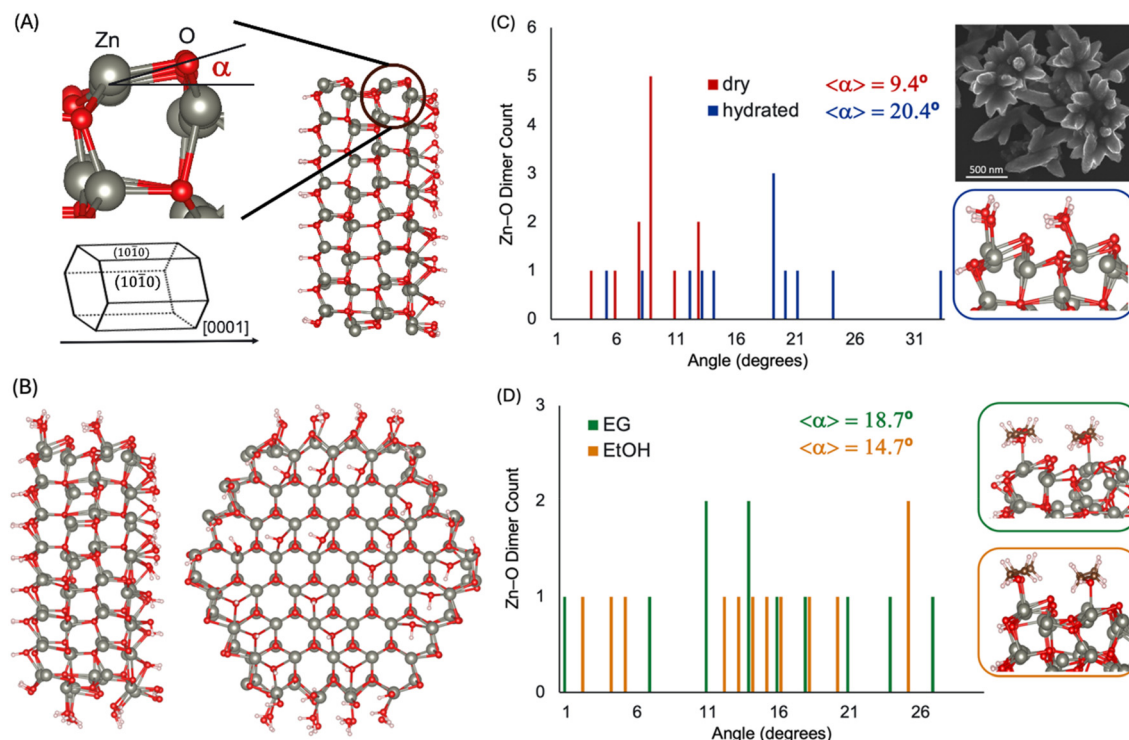
Fig. 1 Solvent effect on the structure of ZnO nanorods. (A) Zn–O dimer relaxation on the (10$\bar{1}$0) surface of ZnO nanoparticle in vacuum. (B) Structure of hydrated (10$\bar{1}$0) and (0001) faces of ZnO nanoparticle. (C and D) Distribution of dipoles on the (10$\bar{1}$0) surface of ZnO nanoparticles in vacuum, and solutions of 2.5 mM Zn(NO$_3$)$_2$/38 mM KOH in water, ethylene glycol, and ethanol. The insets show the structure of the (10$\bar{1}$0) surface of ZnO in the corresponding solvents (full solution structure not shown for clarity). The structure of branched ZnO grown in aqueous solution is shown in the inset in (C).

with two OH-groups per molecule and ethanol (EtOH) with one OH-group were selected to vary the number of bonds between solvent O and surface Zn (up to 2 for each ethylene glycol molecule and 1 for water and ethanol) and hydrogen bonding with neighboring surface oxygen. Both ethylene glycol and ethanol reduce surface dipole compared to that in aqueous solution, with ethylene glycol reducing the average angle for the Zn–O dimers to 18.7° and ethanol to 14.7° (Fig. 1D). These changes in surface dipoles were accompanied by changes in preferential growth direction and the morphology of ZnO particles.

Synthesis of ZnO nanostructures in these solvents was performed by drop-wise addition of 38 mM solution of KOH, which serves as a reducing agent, to the solutions of 2.5 mM Zn(NO$_3$)$_2$ in water, ethylene glycol, and ethanol under identical conditions (see ESI† for details). This procedure keeps the reaction rate approximately the same in all solvents. Thereby, the changes in particle morphology can be mainly attributed to the differences in face-specific barriers for monomer attachment, which define the fast growth directions.

Transmission electron microscopy (TEM) imaging of ZnO crystals grown in aqueous 2.5 mM Zn(NO$_3$)$_2$/38 mM KOH solution revealed a flower-like structure similar to that reported previously[16] (Fig. 2A). The primary particle forms a nanorod along [0001] directions, and the branches form twin bound-

aries with the primary particles and grow predominantly along [0001]. Notably, the concentration-dependent change in the barrier for monomer deposition drives the transition from flower architecture to rod-like branches.[16] The experiments in this study were conducted in the relatively low precursor concentration regime of 2.5 mM Zn(NO$_3$)$_2$, which was expected to produce a flower-like architecture.[16] To test whether impurities affect the growth pathway, precursor solutions were carefully filtered. TEM micrographs show that the morphology did not change in filtered solutions (Fig. 2A, and S1 in the ESI†), supporting the hypothesis that branching in aqueous solutions is driven by the intrinsic properties of ZnO/water interfaces rather than impurity incorporation. The analysis of the initial stages of ZnO growth in aqueous solution revealed that branches form a twin boundary with the primary particle. ZnO branches exhibited elongation along the [0001] direction and slower lateral growth along the [1000] direction (Fig. 2A, second row). The change in solvent from water to ethylene glycol in 2.5 mM Zn(NO$_3$)$_2$/38 mM KOH precursor solution resulted in the preferential growth along the [0001] and [2$\bar{1}$$\bar{1}$0] directions and the formation of (10$\bar{1}$0) plates, and compact, low-aspect ratio nanoparticles were formed in ethanol under identical conditions (Fig. 2B).

Powder XRD of isolated nanoparticles synthesized in these three solvents confirms the solvent-driven change in the rela-
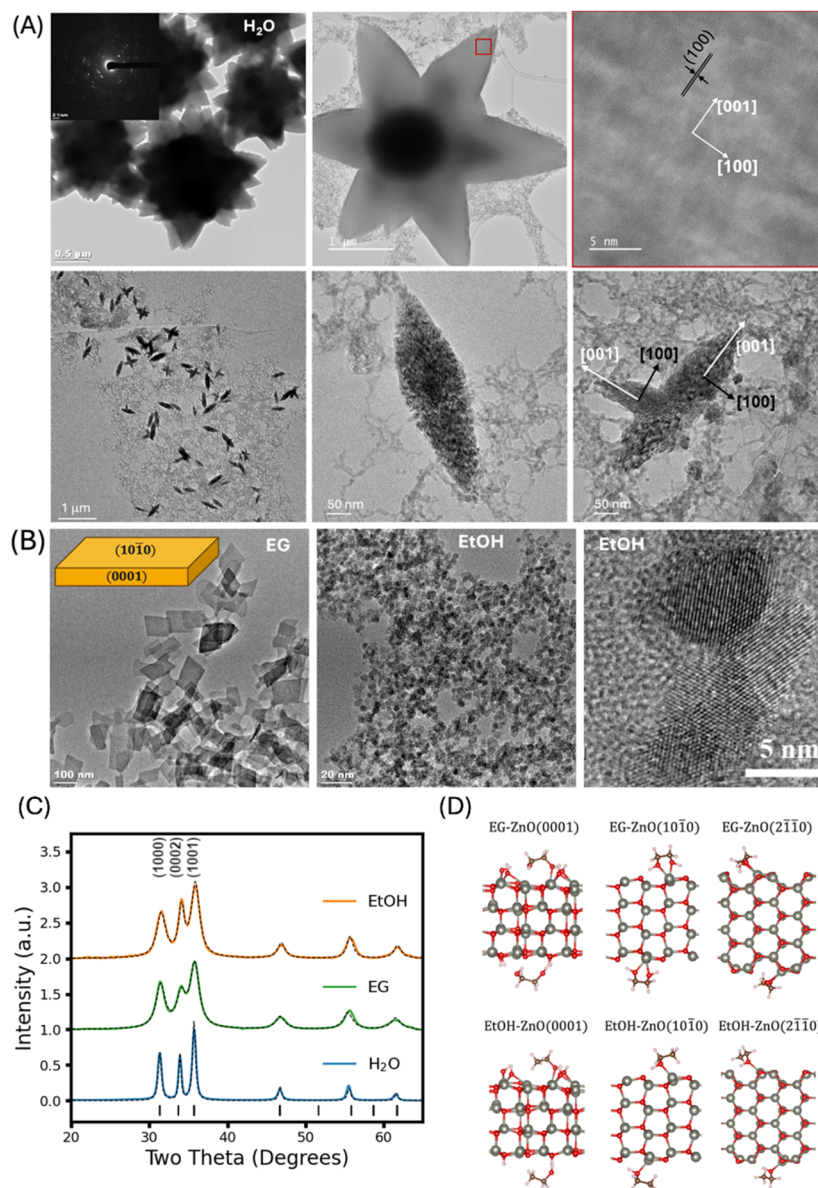
Fig. 2 Solvent effect on the directionality of growth and ZnO particle morphology. TEM micrographs of the morphology of ZnO nanoparticles grown in (A) non-filtered (left) and filtered (middle and right) aqueous solution, (B) ethylene glycol, and ethanol solutions of 2.5 mM $Zn(NO_3)_2$/ 38 mM KOH. The second row in (A) shows the low (left) and high (right) resolution images of the initial stages of particle growth. The schematic of particle morphology in ethylene glycol is shown as an inset. (C) The XRD patterns and corresponding Rietveld fits (dashed lines) of ZnO synthesized in aqueous, ethylene glycol, and ethanol solutions of 2.5 mM $Zn(NO_3)_2$ and 38 mM KOH. (D) Adsorption configuration of ethylene glycol (EG) and ethanol (EtOH) on (0001), (10$\bar{1}$0), and (2$\bar{1}\bar{1}$0) ZnO surfaces.

tive growth directions (Fig. 2C). Relative differences in the primary diffraction peaks at 31.3° (1000), 33.9° (0002), and 35.7° (1001) correlate with the relative differences in the nanoparticles' respective crystal habits. To better quantify these relative differences, these patterns were fit using Rietveld refinement to estimate the preferred axis and anisotropy of the particle aggregates. For ZnO synthesized in H_2O, it was found that the long axis was along the [0001] direction with an anisotropy ratio of 1.5 along this direction. By contrast, ZnO grown in ethylene glycol had an improved match to the experimental pattern when fit to a [10$\bar{1}$0] long axis, with an aniso-

tropic ratio of 0.4, indicating a preference for platelet rather than rod-like morphology. ZnO grown in ethanol was determined to be the most isotropic, with a ratio of 1.1.

Table 1 Solvent binding energy to ZnO faces in eV and the morphology of ZnO particles

	ZnO (0001)	ZnO (10$\bar{1}$0)	ZnO (2$\bar{1}\bar{1}$0)	Morphology
EG	−3.53	−4.95	−3.68	(10$\bar{1}$0) plate
EtOH	−2.85	−3.49	−3.33	Compact

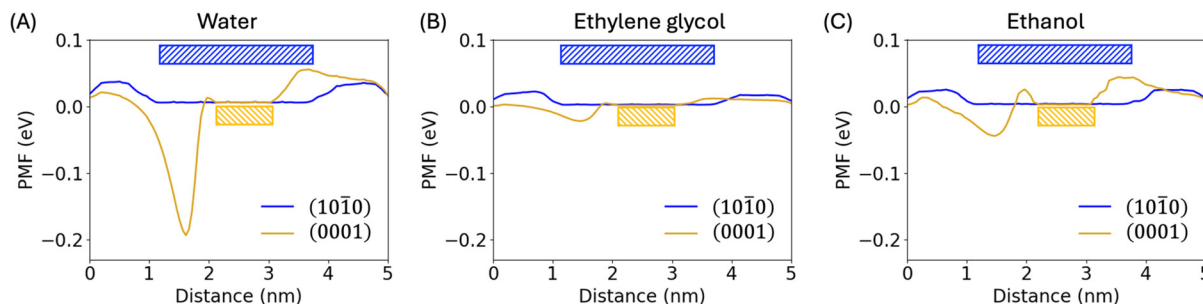**Fig. 3** Solvent effect on the driving forces for Zn-ion deposition onto ZnO surfaces. Potential of mean force of Zn^{2+} ions at (0001) and (10$\bar{1}$0) surfaces of ZnO nanoparticle in 2.5 mM $Zn(NO_3)_2$/38 mM KOH solutions in (A) water, (B) ethylene glycol, and (C) ethanol. Orange and blue rectangles show the position of the (0001) and (10$\bar{1}$0) surfaces of ZnO nanoparticle immersed in electrolyte, respectively.

The strength of solvent adsorption to ZnO crystal faces correlates well with the observed preferential growth directions. The adsorption energy of ethylene glycol to ZnO surfaces is anisotropic, with adsorption energy to (10$\bar{1}$0) face ~1.4 times larger than that to (0001) and (2$\bar{1}\bar{1}$0) faces (Table 1). In contrast, there is little variation between the adsorption energies of ethanol to these ZnO faces (Table 1).

These differences in solvent interactions with ZnO faces reflect the number of binding sites per solvent molecule dictated by the structure of the surfaces and the number of OH groups in the solvent molecules. Ethylene glycol molecule forms 2 bonds with neighboring Zn atoms on the (10$\bar{1}$0) surface, but only 1 bond with surface Zn on (0001) and (2$\bar{1}\bar{1}$0) faces (Fig. 2D). Ethanol molecule forms 1 bond with each of the three surfaces. The binding energies of ethanol two all three ZnO faces are similar to those of ethylene glycol with (0001) and (2$\bar{1}\bar{1}$0) faces, suggesting that the strength of solvent interactions with ZnO faces is largely defined by the solvent OH-group binding with surface Zn.

2.3. Solvent effect on the driving forces for monomer additions and morphological control

The differences in solvent interactions with ZnO faces affect the distribution of precursor ions and their potential of mean force (PMF) at nanoparticle faces, defining the preferential growth direction.

Simulations reveal that in all three solvents considered, there is about $1k_BT$ (where k_BT is the thermal energy, equal to 0.03 eV at a synthesis temperature of 60 °C) barrier for Zn^{2+} deposition onto the (10$\bar{1}$0) surface. However, the PMF of precursor ions at the (0001) surface strongly depends on the solvent (Fig. 3). In water, the PMF has an attractive well of about $7k_BT$ (0.2 eV) and no barrier, indicating a thermodynamic preference for Zn^{2+} attachment to the (0001) surface, which is consistent with the observation that [0001] is the fast growth direction in aqueous solution. The attractive potential well decreases to under $1k_BT$ (0.02 eV) in ethylene glycol and ethanol, and a ~$1k_BT$ (0.03 eV) barrier appears in ethanol (Fig. 3). This dependence of the PMF on the solvent indicates the decrease in the growth preference along [0001] direction in the sequence water > ethylene glycol > ethanol. These differ-

ences in the PMF in these solvents support the observed high uniaxial anisotropy of the growth in water, biaxial 2D growth in ethylene glycol, and isotropic growth in ethanol.

3.   Conclusions

Combined theoretical and experimental studies revealed that interfacial dipolar and solvation forces control the morphology of ZnO crystals during monomer-by-monomer growth. Solvent interactions with crystal faces either reduce or enhance the dipole and control the growth rate of various faces or promote twinning as a dipole compensation mechanism. These findings reflect the nanoscale nature of the particles during nucleation and early stages of growth, which, in the absence of the macroscopic dipole compensation mechanism, elevates dipolar forces to become the main interfacial drives of morphological control. The extension of the finding to other systems can provide a general pathway for ligand-free morphological control of nanoparticles during solution synthesis, enabling the synthesis of well-defined nanomaterials *via* a thermodynamically deterministic pathway.

Author contributions

Duo Song, Lili Liu, Andrew Ritchhart: data curation, formal analysis, investigation, and writing – review & editing. Maria Sushko: conceptualization, supervision, funding acquisition, and writing – review & editing.

Conflicts of interest

The authors declare that they have no known competing financial interests or personal relationships that could have appeared to influence the work reported in this paper.

Data availability

The data supporting the findings of this study are available within the article and/or its ESI.†

Acknowledgements

References

1 V. Pawlik, S. Zhou, S. Y. Zhou, D. Qin and Y. A. Xia, Silver Nanocubes: From Serendipity to Mechanistic Understanding, Rational Synthesis, and Niche Applications, *Chem. Mater.*, 2023, **35**(9), 3427–3449, DOI: **10.1021/acs.chemmater.3c00472**.

2 X. Qi, T. Balankura, Y. Zhou and K. A. Fichthorn, How Structure-Directing Agents Control Nanocrystal Shape: Polyvinylpyrrolidone-Mediated Growth of Ag Nanocubes, *Nano Lett.*, 2015, **15**(11), 7711–7717, DOI: **10.1021/acs.nanolett.5b04204**.

3 W. X. Niu and G. B. Xu, Crystallographic control of noble metal nanocrystals, *Nano Today*, 2011, **6**(3), 265–285, DOI: **10.1016/j.nantod.2011.04.006**.

4 C. Xiao, B. A. Lu, P. Xue, N. Tian, Z. Y. Zhou, X. Lin, W. F. Lin and S. G. Sun, High-Index-Facet- and High-Surface-Energy Nanocrystals of Metals and Metal Oxides as Highly Efficient Catalysts, *Joule*, 2020, **4**(12), 2562–2598, DOI: **10.1016/j.joule.2020.10.002**.

5 T. Sheng, N. Tian, Z. Y. Zhou, W. F. Lin and S. G. Sun, Designing Pt-Based Electrocatalysts with High Surface Energy, *ACS Energy Lett.*, 2017, **2**(8), 1892–1900, DOI: **10.1021/acsenergylett.7b00385**.

6 T. Yu, D. Y. Kim, H. Zhang and Y. N. Xia, Platinum Concave Nanocubes with High-Index Facets and Their Enhanced Activity for Oxygen Reduction Reaction, *Angew. Chem., Int. Ed.*, 2011, **50**(12), 2773–2777, DOI: **10.1002/anie.201007859**.

7 M. S. Jin, H. Zhang, Z. X. Xie and Y. N. Xia, Palladium Concave Nanocubes with High-Index Facets and Their Enhanced Catalytic Properties, *Angew. Chem., Int. Ed.*, 2011, **50**(34), 7850–7854, DOI: **10.1002/anie.201103002**.

8 J. Zhang, M. R. Langille, M. L. Personick, K. Zhang, S. Y. Li and C. A. Mirkin, Concave Cubic Gold Nanocrystals with High-Index Facets, *J. Am. Chem. Soc.*, 2010, **132**(40), 14012–14014, DOI: **10.1021/ja106394k**.

9 Y. T. Shen, S. Su, T. Xu, K. B. Yin, K. S. Yang and L. T. Sun, In Situ Transmission Electron Microscopy Investigation on Oriented Attachment of Nanodiamonds, *Nano Lett.*, 2023, **23**(20), 9602–9608, DOI: **10.1021/acs.nanolett.3c03300**.

10 S. More, B. Joshi, A. Khadka, E. Samuel, Y. I. Kim, A. Aldalbahi, M. El-Newehy, K. Gurav, H. S. Lee and S. S. Yoon, Oriented attachment of carbon/cobalt-cobalt oxide nanotubes on manganese-doped carbon nanofibers for flexible symmetric supercapacitors, *Appl. Surf. Sci.*, 2023, **615**, 156386, DOI: **10.1016/j.apsusc.2023.156386**.

11 Y. L. Li, Y. Wang, J. Q. Wu, Y. Y. Pan, H. Q. Ye and X. P. Zeng, Synthesis of Silver Nanowires Using a Polyvinylpyrrolidone-Free Method with ant Leaf Based on the Oriented Attachment Mechanism, *ACS Omega*, 2023, **8**(2), 2237–2242, DOI: **10.1021/acsomega.2c06481**.

12 F. Y. Li, G. Y. Song, Q. X. Zhang, L. Zhou, J. C. Tai and M. H. Hou, Understanding the growth mechanism of Al-bearing hematite nanoparticles via two-dimensional oriented attachment, *J. Cryst. Growth*, 2023, **620**, 127360, DOI: **10.1016/j.jcrysgro.2023.127360**.

13 D. S. Li, Q. Chen, J. Chun, K. Fichthorn, J. De Yoreo and H. M. Zheng, Nanoparticle Assembly and Oriented Attachment: Correlating Controlling Factors to the Resulting Structures, *Chem. Rev.*, 2023, **123**(6), 3127–3159, DOI: **10.1021/acs.chemrev.2c00700**.

14 M. L. Sushko and K. M. Rosso, The origin of facet selectivity and alignment in anatase TiO2 nanoparticles in electrolyte solutions: implications for oriented attachment in metal oxides, *Nanoscale*, 2016, **8**(47), 19714–19725, DOI: **10.1039/c6nr06953c**.

15 M. L. Sushko, Crystallization pathways and interfacial drivers for the formation of hierarchical architectures, *J. Cryst. Growth*, 2022, **600**, 126914, DOI: **10.1016/j.jcrysgro.2022.126914**.

16 L. L. Liu, M. L. Sushko, E. C. Buck, X. Zhang, L. Kovarik, Z. Z. Shen, J. H. Tao, E. Nakouzi, J. Liu and J. J. De Yoreo, Revisiting, the Growth Mechanism of Hierarchical Semiconductor Nanostructures: The Role of Secondary Nucleation in Branch Formation, *J. Phys. Chem. Lett.*, 2019, **10**(21), 6827–6834, DOI: **10.1021/acs.jpclett.9b02110**.

17 M. Ramya, T. K. Nideep, V. P. N. Nampoori and M. Kailasnath, Solvent assisted evolution and growth mechanism of zero to three dimensional ZnO nanostructures for dye sensitized solar cell applications, *Sci. Rep.*, 2021, **11**(1), 6159, DOI: **10.1038/s41598-021-85701-9**.

18 Y. Ding, Y. Z. Liu, K. C. Pradel, Y. Bando, N. Fukata and Z. L. Wang, Quantifying mean inner potential of ZnO nanowires by off-axis electron holography, *Micron*, 2015, **78**, 67–72, DOI: **10.1016/j.micron.2015.07.008**.

19 J. Y. Kim, M. G. Han, M. B. Lien, S. Magonov, Y. M. Zhu, H. George, T. B. Norris and N. A. Kotov, Dipole-like electro-

static asymmetry of gold nanorods, *Sci. Adv.*, 2018, **4**(2), e1700682, DOI: **10.1126/sciadv.1700682**.

20 M. Yang, K. Sun and N. A. Kotov, Formation and Assembly-Disassembly Processes of ZnO Hexagonal Pyramids Driven by Dipolar and Excluded Volume Interactions, *J. Am. Chem. Soc.*, 2010, **132**(6), 1860–1872, DOI: **10.1021/ja906868h**.

21 Y. Guyodo, A. Mostrom, R. L. Penn and S. K. Banerjee, From Nanodots to Nanorods: Oriented aggregation and magnetic evolution of nanocrystalline goethite, *Geophys. Res. Lett.*, 2003, **30**(10), 1512, DOI: **10.1029/2003gl017021**.

22 S. Mukherjee, S. Pramanik, S. Das, S. Chakraborty, S. Mondal, T. Ghosh, R. Nath and P. K. Kuiri, Oriented attachment induced morphology modulation of ZnO nano-particles at low temperature using KOH as a morphology controller, *New J. Chem.*, 2021, **45**(36), 17009–17024, DOI: **10.1039/d1nj02248b**.

23 S. Dag, S. Z. Wang and L. W. Wang, Large Surface Dipole Moments in ZnO Nanorods, *Nano Lett.*, 2011, **11**(6), 2348–2352, DOI: **10.1021/nl200647e**.

24 D. Song, E. J. Bylaska, K. M. Rosso and M. L. Sushko, Role of Dynamic Polarization Interactions in the Electrical Double Layer at Calcite (104) Interfaces with Aqueous Solutions, *J. Phys. Chem. C*, 2024, **128**(13), 5686–5696, DOI: **10.1021/acs.jpcc.3c07837**.

25 D. Song, M. L. Sushko, E. J. Bylaska and K. M. Rosso, Development and Application of Hybrid AIMD/cDFT Simulations for Atomic-to-Mesoscale Solutions and Reactions, *J. Chem. Phys.*, 2024, **160**, 064112, DOI: **10.1063/5.0190686**.

26 F. Decremps, F. Datchi, A. Saitta, A. Polian, S. Pascarelli, A. Di Cicco, J. Itié and F. Baudelet, Local structure of condensed zinc oxide, *Phys. Rev. B:Condens. Matter Mater. Phys.*, 2003, **68**(10), 104101, DOI: **10.1103/PhysRevB.68.104101**.

27 M. Goano, F. Bertazzi, M. Penna and E. Bellotti, Electronic structure of wurtzite ZnO: Nonlocal pseudopotential and ab initio calculations, *J. Appl. Phys.*, 2007, **102**(8), 083709, DOI: **10.1063/1.2794380**.